Flow investigation of multiphase manganese slags

Vishal Rimal[1], *and Merete Tangstad*[2]

1. PhD candidate, Department of Materials Science and Engineering, Norwegian University of Science and Technology (NTNU), Trondheim, Norway. Email: vishal.rimal@ntnu.no
2. Professor, Department of Materials Science and Engineering, Norwegian University of Science and Technology (NTNU), Trondheim, Norway. Email: merete.tangstad@ntnu.no

Keywords: manganese, multiphase, slag, flow

ABSTRACT

Multiphase slags form the basis of the reduction pathway for manganese ferroalloy production. The present work aims to understand the flow of slag through the coke bed based on experimentation in controlled conditions. Synthetic slags of different basicities were evaluated for their phase composition, viscosity, and flow. The two-phase slag will have two zones: a liquid slag zone and a multiphase zone. The multiphase zone will consist mostly of a solid phase with some liquid slag between the solid particles. The multiphase part will hence have a high viscosity. The liquid zone will flow into the coke bed while the multiphase area will stay. With increasing reduction, the multiphase area will decrease in size until the solid phase is gone and the whole slag will flow into the coke bed. The effective viscosity of slag will decrease with the lowering of the solid oxide phase. The results from flow experiments confirmed that the segregation of phases occurs when slag flows through the coke bed. It is observed that the flow is dependent both on the size of the void and the viscosity of slag.

INTRODUCTION

High-carbon ferromanganese are alloys containing Fe and C with a major proportion of Mn. They are produced by the carbothermic reduction of oxidic raw materials using coke in a submerged arc furnace (SAF). The SAF has two main reaction zones, (i) pre-reduction zone and (ii) reduction zone. In the pre-reduction zone, CO reduces iron oxides to metallic iron and higher Mn oxides to solid MnO. Carbonates will also decompose to basic oxides. Gas reduction of MnO to Mn is not possible due to the high stability of MnO. In the reduction zone, the pre-reduced components meet the coke bed. A slag mixture of liquid and solid phases is formed at this stage. The liquid phase consists of CaO, MnO, MgO, Al_2O_3, and SiO_2. The solid phase occurs due to the saturation of MnO in the liquid phase. The MnO present in the liquid phase reacts with the C in the coke bed through the following reaction to yield metallic Mn:

$$MnO_{liquid\ slag} + C_{solid} = Mn_{liquid} + CO_{gas}$$

As the reaction proceeds, the solid phase decreases and the reaction will rapidly slow down when a single-phase slag is achieved (Kumar, Ranganathan and Sinha, 2007; Tangstad *et al.*, 2021; Hockaday, Dinter and Reynolds, 2023; Larssen and Tangstad, 2023).

In a SAF the coke bed does not act as a source of fuel rather it provides the carbon reductant, but more importantly the electrical resistance for energy development (Davies *et al.*, 2023). The flow behaviour of the slag into the coke bed significantly affects the efficiency and the environmental emissions in the SAF (Oh and Lee, 2016). A consistent flow with characteristic fluid behaviour is desired for the smooth operation of SAF (Natsui *et al.*, 2020; Dong *et al.*, 2021). The coke bed can be described as a packed bed with the coke particles acting as the packing material. The packing is random and generally results in the formation of interconnected voids of variable sizes through which the liquids trickle down and gases flow upwards. The coke bed should be permeable to allow the flow of the different phases. The structure of the packed bed and packing density affects the size of voids, their interconnectivity as well as the permeability and liquid holdup (Geleta, Siddiqui and Lee, 2020; Natsui *et al.*, 2021).

The flow of fluids through the coke bed is often interpreted in terms of void, micro-, and macro-scales. The majority of the studies on relations affecting the flow of slag have been based on cold models and non-moving packed beds, so inferences in high-temperature real-world conditions can vary significantly. Manuscripts have generally considered the coke bed as stationary since the descent of coke bed is very slow (Fukutake and Rajakumar, 1982). A number of studies at high temperatures have been reported, however, the inconsistent physical and chemical properties of coke make it difficult to generalize the characteristics like reactivity, wetting, and strength (Safarian and Tangstad, 2009; George *et al.*, 2014). The liquid slag/metal often flows as droplets or channels in the coke bed (Jeong, Kim and Sasaki, 2014). The size of voids has been found to influence the rate of flow of liquids as it progresses through the coke bed (George *et al.*, 2014). Prior studies have shown that the overall resistance to the liquid flow increases with the decrease in particle size in the packed bed (Bando *et al.*, 2005; Kawabata, Liu, *et al.*, 2006; Kawabata, Shinmyou, *et al.*, 2006).

For manganese ferroalloys, a significant portion of reduction generally takes place at the top section of the coke bed. The charge (oxides and coke) will settle on top of the permanent coke bed. The

proportion of coke fed into the furnace will determine if the permanent coke bed is consumed in the process or not. The charge provides the necessary carbon source. According to theory, negligible reduction takes place when the slag has entered the coke bed as a single phase since the activity of MnO is very low when a single-phase slag is achieved (Olsen, Tangstad and Lindstad, 2007). The interaction of slag with the coke bed is thus dependent on the reduction of Mn in the upper sections of the coke bed.

The flow of slag through the coke bed will depend on the size of voids and the viscosity of Mn slag. The viscosity of Mn slag is high when the slag exists as a solid-liquid mixture and decreases with a decrease in the proportion of solid phase. When the melt initially encounters the coke bed, the viscosity of slag is high. As the reduction proceeds the viscosity decreases enabling the flow of slag through the coke bed (Tang and Tangstad, 2007; Muller, Zietsman and Pistorius, 2015).

This manuscript aims to understand the flow of slag in controlled conditions under the influence of gravity. Limited literature exists elucidating the Mn slag behaviour in the coke bed. The specific interest here is thus to comprehend the segregation of phases as the reduction proceeds and to find the parameters that affect the flow of slag.

EXPERIMENTAL DETAILS

Materials

MnO, SiO_2, Fe_2O_3, CaO, MgO, Al_2O_3, and CaS of analytical grade were procured from Sigma Aldrich and used as received. Double distilled water was used for the preparation of briquettes. Two types of graphite substrates were used for the experiments: (i) flat, and (ii) funnel (Figure 1). The flat substrate was used to evaluate the phase composition and thus calculate the viscosity. The funnel substrate was used to comprehend the flow of slag under the influence of gravity.

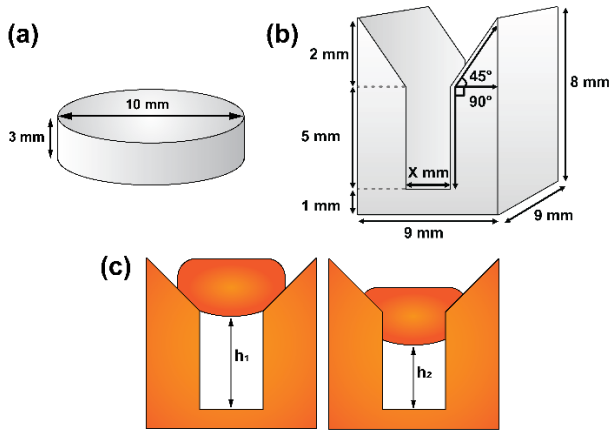

FIGURE 1 – Illustration of (a) Flat graphite substrate, (b) Graphite funnel diameter "X = 2, 3, 4, 6 mm," (c) Displacement measurement protocol used in this study. Drawing not to scale.

Methodology

Synthetic slags of different basicity were prepared based on the ratio of chemical compounds as shown in Table 1. The basicity B, in this manuscript is defined using a wt% basis as

$$B = \frac{CaO + MgO}{SiO_2 + Al_2O_3}$$

The compounds "as received" were mixed, briquetted using a press, and allowed to dry overnight. The samples were then placed on the graphite substrate and heated in a sessile drop furnace in an

inert atmosphere with Ar airflow at 0.1 L/min. The heating rate was set at 300 °C/min till 900 °C followed by 50 °C/min till 1500 °C. The experiments were independently done for different holding durations (0 min, 20 min, 60 min, and 120 min) at 1500 °C as shown in Figure 2. Additionally, slag was also prepared by (i) grinding the mixture before heating as well as by (ii) using a master slag powder of SiO_2, CaO, MgO, Al_2O_3, and CaS prepared at 1700 °C. It was observed that identical slags were produced in all three routes. The master slag route was used for all experiments in this manuscript. The basicity was adjusted by adding additional SiO_2 to the mixture before heating.

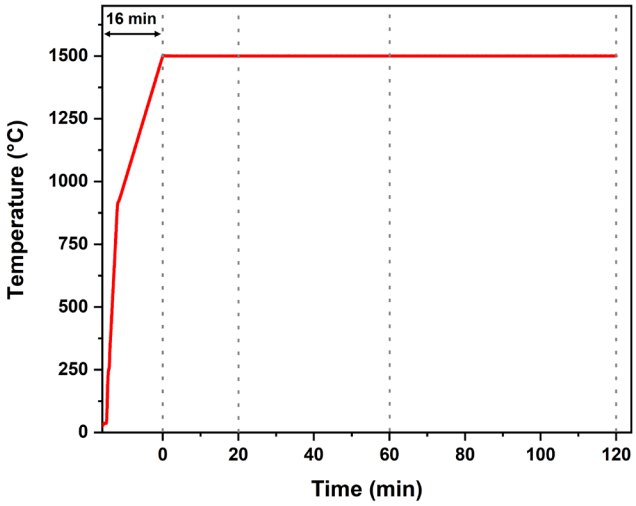

FIGURE 2 – Heat profile for experiments.

The proportions of the different phases were found from picture analyses from SEM micrographs. The area covered by the different phases was calculated using the measurement feature in Adobe Photoshop 2023. The flow was estimated from the wetting images by evaluating the y-axis displacement of the slag mixture with respect to the centre of the graphite funnel as shown in Figure 1c. The flow measurements were made till the completion of flow or 2 hours of holding (whichever preceded earlier).

TABLE 1 – Chemical composition of reactants used for experiments.

Basicity	Compound (%)						
	MnO	SiO_2	Fe_2O_3	CaO	MgO	Al_2O_3	CaS
0.8	72.86	10.28	7.85	7.26	1.27	0.30	0.17
1	70.31	9.71	9.31	8.60	1.51	0.36	0.20
1.22	76.45	6.69	7.85	7.26	1.27	0.30	0.17

Apparatus

A sessile drop furnace equipped with a pyrometer and a C-type thermocouple was used for heating the samples. The wetting images were taken using a digital video camera (Allied Vision Prosilica GT2000, Edmund Optics, Inc., Barrington) with a telecentric lens (Navitar 1-50993D) at a resolution of 2048×1088 pixels. The distribution of different phases was obtained from SEM (Zeiss Ultra 55LE) images. The images were recorded at 200x magnification with an accelerating voltage of 10 kV. Due to the dimensional limitations, multiple images were captured to cover the periphery of the sample and subsequently compiled into a single image. EPMA (JEOL JXA-8500) was used for determining the composition.

RESULTS AND DISCUSSION

Phase composition and viscosity

The phase composition and viscosity were studied for a basicity of 0.8 and 1.22 on a flat substrate for different durations of holding i.e., 0 min, 20 min, 60 min, and 120 min at 1500 °C. For all the holding durations, three phases viz. liquid slag phase containing MnO-CaO-Al_2O_3-MgO and SiO_2, solid slag phase containing mainly MnO, and reduced Mn-Fe-metal could be observed in the SEM images (Figure 3). SEM image showing the solid particles surrounded by the liquid phase as well as the dendrites in the liquid slag, which are assumed to be the MnO phase precipitated during cooling is shown in Figure 4. The amount of solid phase was found to decrease with time as the reduction of MnO progressed. The composition analysis obtained using WDS/EPMA shows that the %MnO in the liquid phase is higher for 0.8 basicity (Figure 5). For the solid phase, the %MnO is the same for both basicities and close to 90%. Here the solid phase does not include dendrites. The composition remains constant throughout holding for both phases except values at 0 min being found to deviate from others. The region has been highlighted in grey in the figure and represents the uncertainty in values in the studied range. Subsequent plots also have similar deviations at 0 min holding and are highlighted similarly. The %MnO in the liquid phase was also plotted against basicity (Figure 6). It is seen that the %MnO in liquid slag increases with a decrease in basicity. The experimental values were lower than theoretical predictions, however, the trend is comparable.

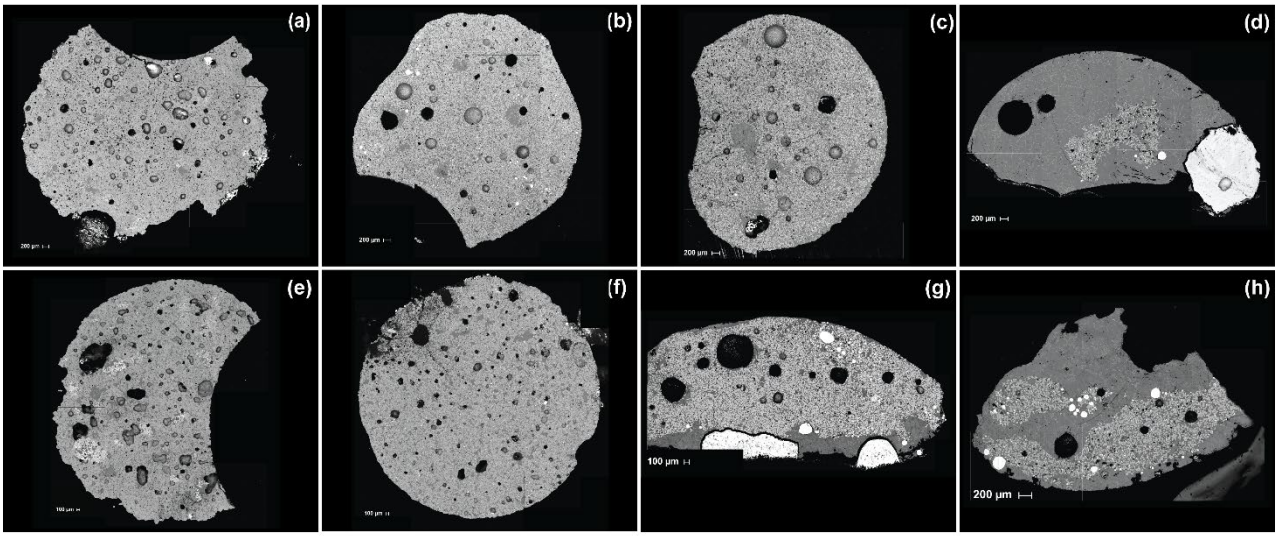

FIGURE 3 – SEM imaging of (a) 0.8 basicity at 0 min, (b) 0.8 basicity at 20 min, (c) 0.8 basicity at 60 min, (d) 0.8 basicity at 120 min, (e) 1.22 basicity at 0 min, (f) 1.22 basicity at 20 min, (g) 1.22 basicity at 60 min, (h) 1.22 basicity at 120 min.

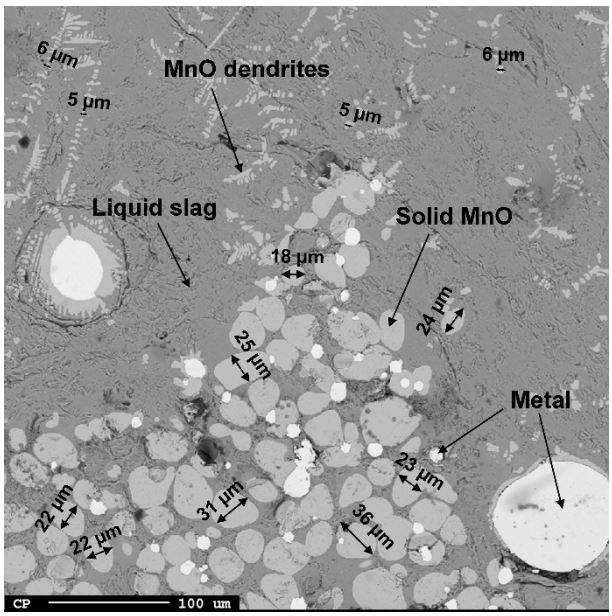

FIGURE 4 – SEM image showing the different phases. In the lower part one can see the multiphase, the mixture of solid MnO particles in a liquid, and in the top part the liquid.

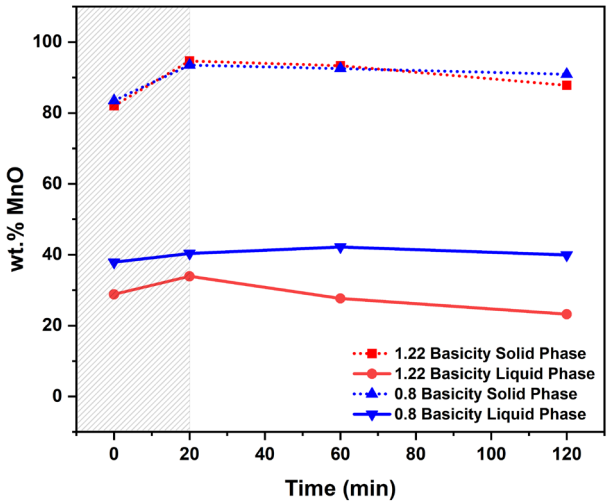

FIGURE 5 – wt.% MnO vs. Time for both solid MnO phase and liquid phase.

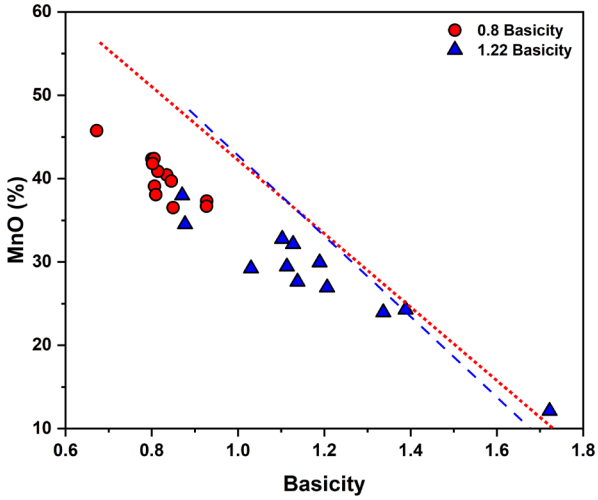

FIGURE 6 – %MnO vs. Basicity (red and blue line indicate theoretical trend for 0.8 basicity and 1.22 basicity respectively).

The phase distribution is presented in Figure 7. As explained in the preceding paragraph, the solid phase decreases with reduction, that is the holding time. Using the phase distribution data, the overall MnO content was calculated using the formula:

$$\%MnO = \theta_{solid} \cdot \%MnO_{solid} + \theta_{liquid} \cdot \%MnO_{liquid}$$

where, %MnO = total MnO content, θ_{solid} = fraction of solid phase, $\%MnO_{solid}$ = %MnO in the solid phase, θ_{liquid} = fraction of liquid phase, and $\%MnO_{liquid}$ = %MnO in the liquid phase. Figure 8 shows the rate of MnO reduction with respect to time for 0.8 and 1.22 basicity. The rate of MnO reduction is constant for both basicities. The reduction of MnO is highly endothermic and literature suggests that the rate of reduction is chemically controlled and not transport-controlled (Ostrovski *et al.*, 2002; Olsen, Tangstad and Lindstad, 2007). The present result counters earlier reports wherein the rate of reduction was found to be lower for high basicity solid-liquid mixture. Reports have also concluded that higher basicity was found to give a faster reduction in the case of a homogenous single-phase slag (Olsø, Tangstad and Olsen, 1998).

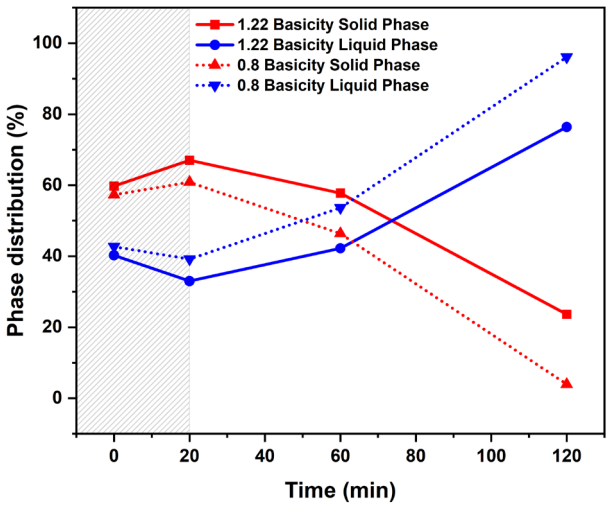

FIGURE 7 – Calculated amount of solid MnO phase and liquid phase.

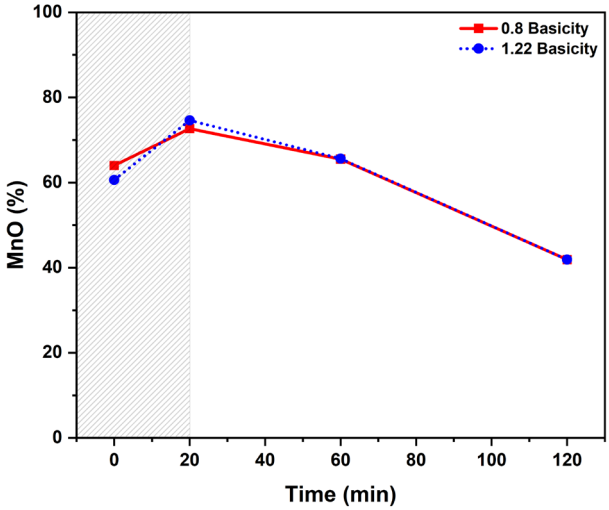

FIGURE 8 – Total %MnO vs. Time showing the reduction of slag with time.

The viscosity of the liquid slag phase was calculated using the Urbain model developed by Mills et al. (Mills, Yuan and Jones, 2011). Figure 10 shows the viscosity of the liquid phase for 0.8 and 1.22 basicity at 0 min and 120 min of holding. The experimental composition at 1500°C was also extended for viscosity calculation at 1400 °C and 1600 °C. The effect of temperature on viscosity was well-defined in the model used. In the absence of a solid phase, the viscosity is higher for low-basicity

systems and vice versa. However, for systems with a solid phase in existence the effective viscosity will have to be described using the Einstein-Roscoe equation (Roscoe, 1952):

$$\mu e \ = \ \mu(1 - 1.35\theta)^{-(\frac{5}{2})}$$

where, μ_e = effective viscosity of the slag, μ = viscosity of liquid phase, and θ is the fraction of precipitated solid phases. It is found that for a solid-liquid mixture, the effective viscosity is higher for high basicity systems as it contains a higher amount of solid MnO and the viscosity gradually lowers with lowering the amount of solid phase (Figure 11). For this calculation, the entire sample has been considered as a mixture of liquid and solid phases. Upon attainment of homogenous slag, the viscosity trend will reverse as discussed earlier.

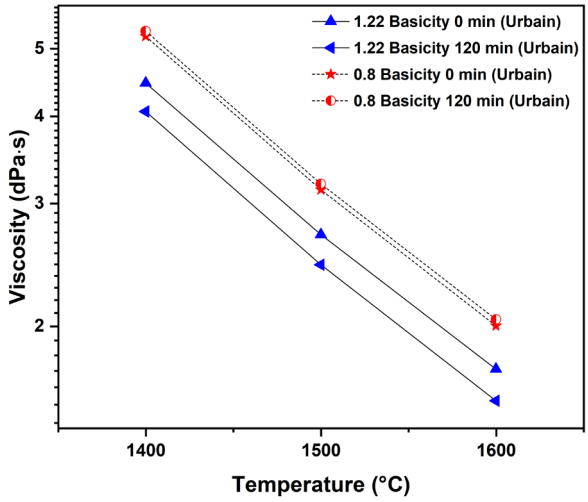

FIGURE 9 – Viscosity of liquid slag at different temperatures.

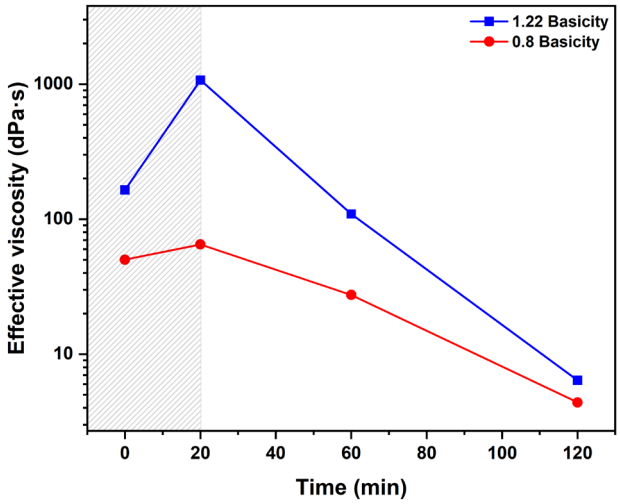

FIGURE 10 – Effective viscosity vs. Time.

The effective density of the slag was also determined using the equation:

$$\rho \ = \ \frac{(m_1 + m_2)}{(V_1 + V_2)}$$

where, ρ = effective density, m_1 = mass of solid phase, m_2 = mass of liquid phase, V_1 = volume of solid phase, and V_2 = volume of liquid phase. The effective density of the slag mixture was found to be roughly constant for 0.8 and 1.22 basicity at different holding durations (Figure 12). The effective density of the slag mixture lowers with the decrease in the solid phase.

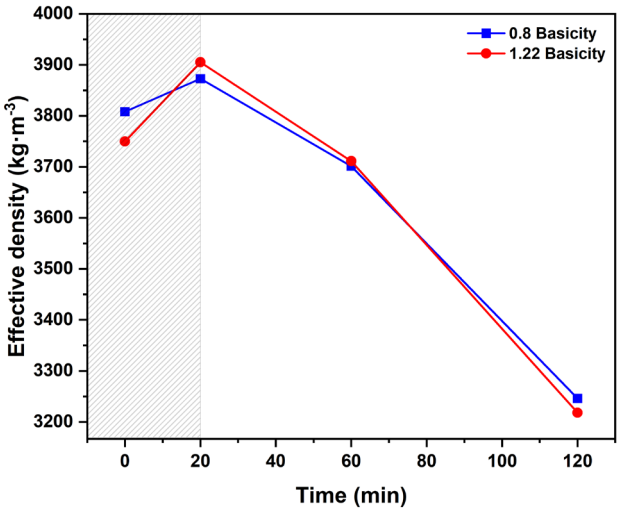

FIGURE 11 – Effective density vs. Time.

Flow measurement

Slags of three different basicities (0.8, 1, and 1.22) were evaluated using the funnel substrate to replicate the flow of slag through the coke bed in controlled conditions under the influence of gravity. The funnels of varying dimensions represent the different void sizes in the coke bed. The upper portion of the funnel represents the neck of the voids in the coke bed. The samples were heated using the same temperature profile as the flat substrate. Figure 13 shows the displacement of slag with respect to time at a constant temperature of 1500 °C. The time ranges from 0 to 120 min of holding. The duration to complete the flow was typically quicker for funnels with larger dimensions like 3 mm and 4 mm. The slowest flow was observed for samples studied in 2 mm funnels for all basicities. This indicates that the flow of slag is influenced by the size of voids in the coke bed.

The live images obtained from the sessile drop furnace have been superimposed in the displacement plots (Figure 13). The reduction proceeds from the slag surface in contact with carbon and the produced metal phase typically appears away from the slag-carbon interface, here in our case the top or bottom portion of the funnel. The low-viscosity and higher-density metal phase is immiscible in the slag phase and separates as droplets that accumulate together resulting in a larger metal phase. Correlating the images and displacement, the metal phase is thus assumed to bring the sudden rapid displacement in the studied plots.

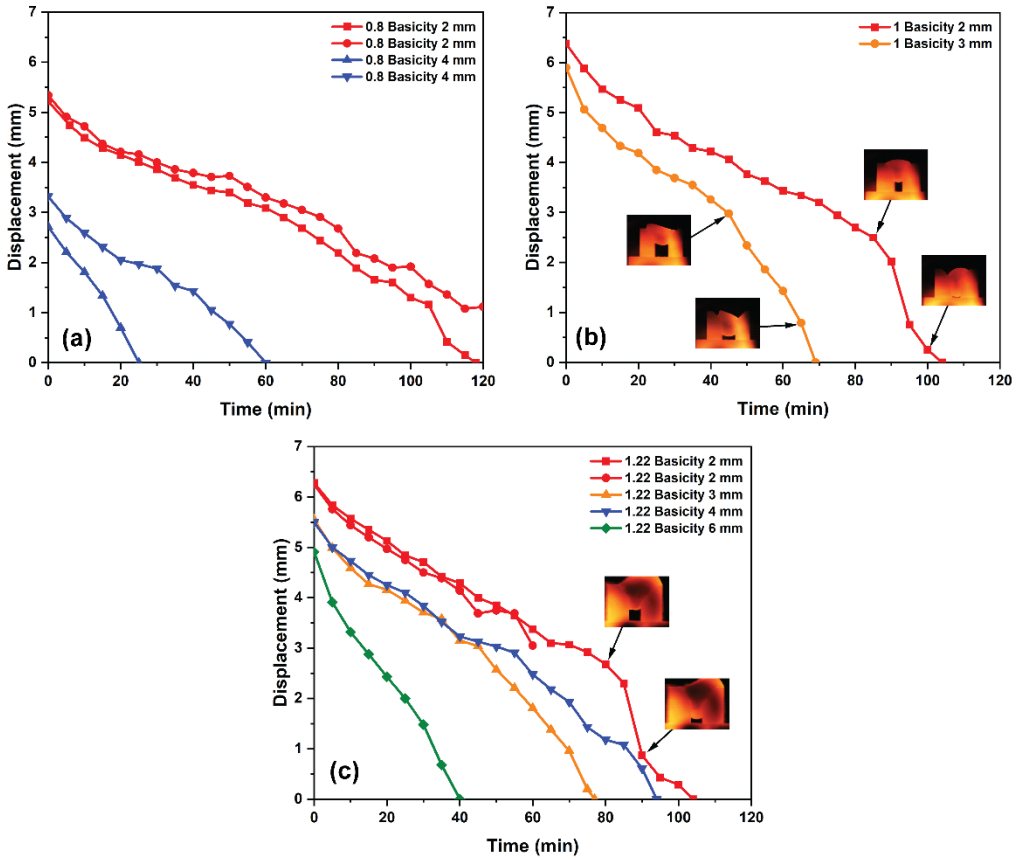

FIGURE 12 – Displacement vs. Time plots for different basicity and funnel dimensions.

SEM images of the funnels after completion of flow show the presence of solid, liquid, and metal phases (Figure 14). It is however observed that the phases segregate as the reduction proceeds. The slag is seen to comprise of two regions: a homogenous liquid slag of low viscosity and a multiphase solid-liquid mixture possessing high viscosity. The segregation pattern thus follows the trend of the multiphase slag at the top, homogenous slag in the middle, and metal phase at the bottom of the funnel. The region covered by the multiphase slag has high viscosity, which limits it from deforming. The low viscosity of the homogenous liquid slag allows it to seep under the multiphase region despite possessing a lower density. The immiscibility between the metal and liquid slag results in the clear demarcation between the two phases. A major portion of the metal phase is found at the bottom section of the funnel. However, it could be seen that in situations where the metal phase is produced in the upper sections of the funnel, the metal phase is unable to pass through the multiphase region. The viscosity of the multiphase region can be said to have a considerable impact on determining the flow of slag as it proceeds through the coke bed.

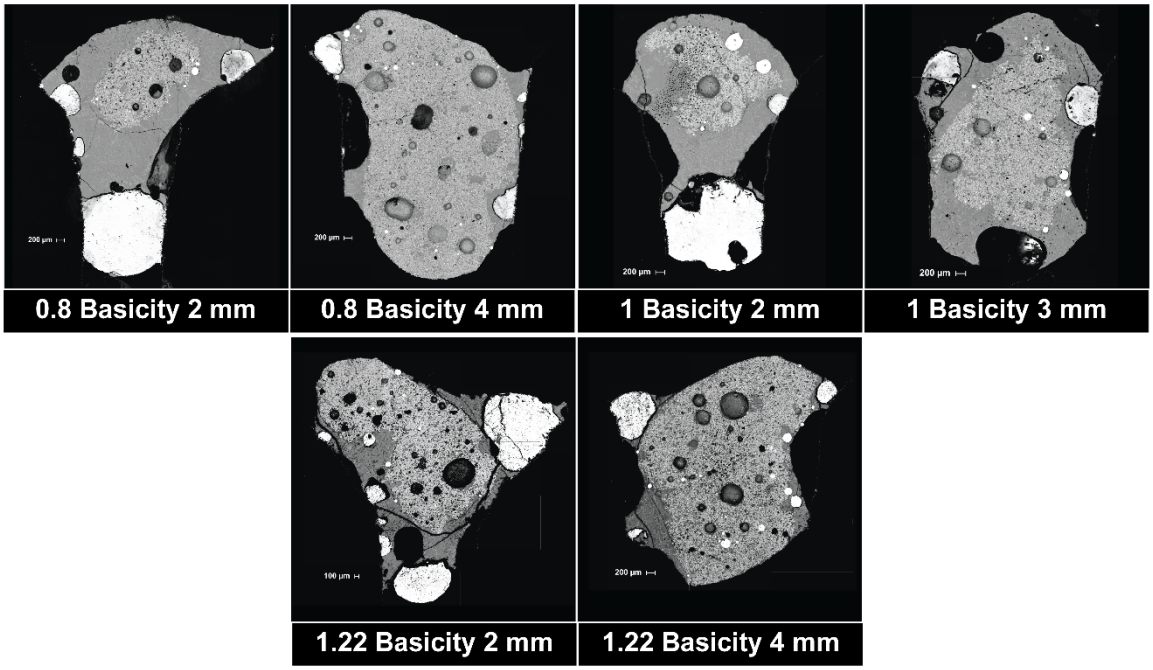

FIGURE 13 – SEM images of the different funnels after completion of flow.

As previously discussed, the proportion of solid phase decreases with increasing Mn reduction over time. It is seen in SEM images that for the samples investigated in funnel experiments, the quicker flow is generally accompanied with a greater fraction of multiphase. For the 2 mm funnels, the amount of multiphase is considerably less compared to 3 mm and 4 mm funnels. One presumption for this inference is that the dimension of the viscous multiphase in 2 mm is larger than the lower portion of the funnel, which prevents the slag from flowing and enables the reduction to proceed for longer durations. For 4 mm funnels, the multiphase region slides down enabling quick flow, accompanied with low reduction. Figure 15 shows the total %MnO after completion of flow for the studied funnels. The %MnO is greater for 4 mm funnel compared to 2 mm funnel for all basicities, which confirms the lowering in reduction with an increase in the size of funnels. It can be mentioned that 3 mm with 1.22 basicity is an outliner from this theory.

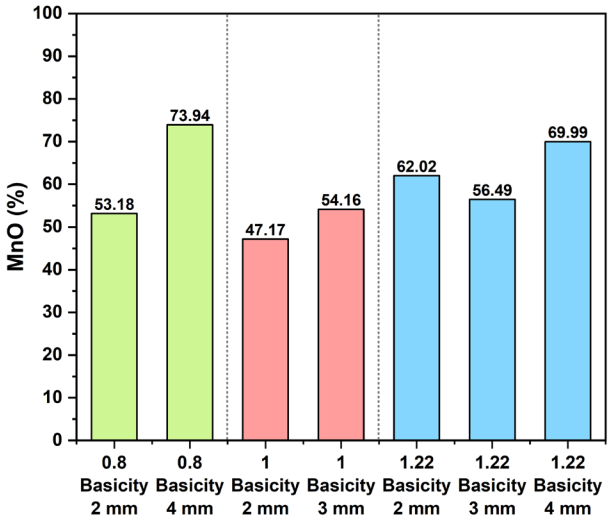

FIGURE 14 – Total %MnO for different basicities and funnel sizes.

The flow of Mn slag through the coke bed thus has two prime factors affecting its flow: (i) dimension of void neck, and (ii) the viscosity of slag. As discussed in the previous section, the flow rate increases with the increase in size of voids. For Mn slag, the high viscosity slag at first encounters the top or outline of the coke bed. Initially, the flow will be extremely difficult even for big void neck dimensions primarily because the viscous forces will dominate and prevent the flow. As the reduction

proceeds the metal phase would trickle down as droplets and eventually result in a metal phase with a clear demarcation with the slag phase. The multiphase slag on the other hand is unable to flow unless the void neck is larger than the multiphase volume at the neck. However, the homogeneous slag (with low viscosity) that is produced during the process drains into the voids. The situation is depicted in Figure 16. If the void neck is large enough to allow the multiphase to flow, this will result in a highly viscous slag being taken into the coke bed making it even more detrimental for smooth flow. Previous excavations have put explanations that the reduction generally completes at the upper sections and the coke bed is generally devoid of significant multiphase slag presence making the large void neck situation unlikely to be encountered in practical scenarios. The type of coke and ash percent are also influential during the flow of slags inside the coke bed however for Mn slag, the viscosity, wetting, and size of voids will most likely be the prime criterion that need to be optimized before other factors are taken into consideration.

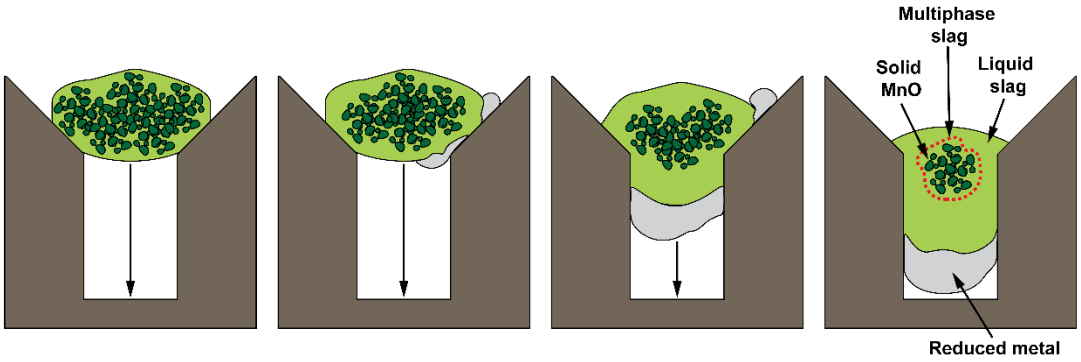

FIGURE 15 – Flow of slag in FeMn production.

Correlating with the discussion in the introduction, it can be safely concluded that the reduction generally proceeds at the top section of the coke bed in the presence of small voids. A single-phase slag and metal phase is anticipated inside the coke bed. The presence of small voids results in minimum reduction taking place inside the coke bed, but the majority on top of the coke bed.

CONCLUSION

The reduction rate was found to be constant for the studied basicity. The effective viscosity and density decrease with the lowering of the proportion of solid phase. The flow of slag was found to be influenced by the size of funnels, indicating that void size in the coke bed is an important parameter influencing the flow. It can be concluded that a slower flow is expected for coke bed with smaller voids. As the slags flow, the segregation of phases takes place. The solid-liquid multiphase possesses a distinct viscous character. For small voids, the multiphase is unable to flow until a substantial amount of solid phase is reduced whilst a larger void will result in quick flow at the expense of any substantial reduction.

ACKNOWLEDGEMENTS

This publication is funded by the Norwegian Research Council through the KPN project Recursive (326581), and the authors gratefully acknowledge the financial support received.

CONFLICT OF INTEREST

On behalf of all authors, the corresponding author states that there is no conflict of interest.

REFERENCES

Bando, Y. *et al.* (2005) 'Effects of packed structure and liquid properties on liquid flow behavior in lower part of blast furnace', *ISIJ International*, 45(10), pp. 1461–1465. Available at: https://doi.org/10.2355/isijinternational.45.1461.

Davies, J. *et al.* (2023) 'Pre-reduction of United Manganese of Kalahari Ore in CO/CO2, H2/H2O, and H2 Atmospheres', *Metallurgical and Materials Transactions B*, 54(2), pp. 515–535.

Dong, X.F. *et al.* (2021) 'Investigation of Molten Liquids Flow in the Blast Furnace Lower Zone: Numerical Modelling of Molten Slag Through Channels in a Packed Bed', *Metallurgical and Materials Transactions B: Process Metallurgy and Materials Processing Science*, 52(1), pp. 255–266. Available at: https://doi.org/10.1007/s11663-020-02009-1.

Geleta, D.D., Siddiqui, M.I.H. and Lee, J. (2020) 'Characterization of Slag Flow in Fixed Packed Bed of Coke Particles', *Metallurgical and Materials Transactions B: Process Metallurgy and Materials Processing Science*, 51(1), pp. 102–113. Available at: https://doi.org/10.1007/s11663-019-01750-6.

George, H.L. *et al.* (2014) 'Flow of molten slag through a coke packed bed', *ISIJ International*, 54(4), pp. 820–826. Available at: https://doi.org/10.2355/isijinternational.54.820.

Hockaday, S.A.C., Dinter, F. and Reynolds, Q.G. (2023) 'The thermal decomposition kinetics of carbonaceous and ferruginous manganese ores in atmospheric conditions', *Journal of the Southern African Institute of Mining and Metallurgy*, 123(8), pp. 391–398. Available at: https://doi.org/10.17159/2411-9717/2527/2023.

Jeong, I.H., Kim, H.S. and Sasaki, Y. (2014) 'Trickle flow behaviors of liquid iron and molten slag in the lower part of blast furnace', *Tetsu-To-Hagane/Journal of the Iron and Steel Institute of Japan*, 100(8), pp. 925–934. Available at: https://doi.org/10.2355/tetsutohagane.100.925.

Kawabata, H., Liu, Z., *et al.* (2006) 'Characteristics of liquid hold-ups in a soaked and unsoaked fixed bed', *Tetsu-To-Hagane/Journal of the Iron and Steel Institute of Japan*, 92(12), pp. 885–892. Available at: https://doi.org/10.2355/tetsutohagane1955.92.12_885.

Kawabata, H., Shinmyou, K., *et al.* (2006) 'Influence of channeling factor on liquid hold-ups in an initially unsoaked bed', *Tetsu-To-Hagane/Journal of the Iron and Steel Institute of Japan*, 92(12), pp. 893–900. Available at: https://doi.org/10.2355/tetsutohagane1955.92.12_893.

Kumar, M., Ranganathan, S. and Sinha, S.N. (2007) 'Kinetics of reduction of different manganese ores', in *Innovations In The Ferro Alloy Industry - Proceedings of the XI International Conference on Innovations in the Ferro Alloy Industry, Infacon XI*, pp. 241–246.

Larssen, T.A. and Tangstad, M. (2023) 'Effect of Raw Materials on Temperature Development during Prereduction of Comilog and Nchwaning Manganese Ores', *Minerals*, 13(7), p. 920.

Mills, K.C., Yuan, L. and Jones, R.T. (2011) 'Estimating the physical properties of slags', *Journal of the Southern African Institute of Mining and Metallurgy*, 111(10), pp. 649–658.

Muller, J., Zietsman, J.H. and Pistorius, P.C. (2015) 'Modeling of Manganese Ferroalloy Slag Properties and Flow During Tapping', *Metallurgical and Materials Transactions B: Process Metallurgy and Materials Processing Science*, 46(6), pp. 2639–2651. Available at: https://doi.org/10.1007/S11663-015-0426-7/FIGURES/14.

Natsui, S. *et al.* (2020) 'Numerical study of binary trickle flow of liquid iron and molten slag in coke bed by smoothed particle hydrodynamics', *Processes*, 8(2). Available at: https://doi.org/10.3390/pr8020221.

Natsui, S. *et al.* (2021) 'Comprehensive numerical assessment of molten iron–slag trickle flow and gas countercurrent in complex coke bed by Eulerian–Lagrangian approach', *Chemical Engineering Journal*, 414(January), p. 128606. Available at: https://doi.org/10.1016/j.cej.2021.128606.

Oh, J.S. and Lee, J. (2016) 'Composition-dependent reactive wetting of molten slag on coke substrates', *Journal of Materials Science*, 51(4), pp. 1813–1819. Available at: https://doi.org/10.1007/s10853-015-9588-6.

Olsen, S.E., Tangstad, M. and Lindstad, T. (2007) 'Production of manganese ferroalloys', p. 247.

Olsø, V., Tangstad, M. and Olsen, S.E. (1998) 'Reduction kinetics of MnO-saturated slags', *8th International Ferroalloys Congress*, 8, pp. 279–283.

Ostrovski, O. *et al.* (2002) 'Kinetic modelling of MnO reduction from manganese ore', *Canadian Metallurgical Quarterly*, 41(3), pp. 309–318. Available at: https://doi.org/10.1179/cmq.2002.41.3.309.

Roscoe, R. (1952) 'The viscosity of suspensions of rigid spheres', *British Journal of Applied Physics*, 3(8), pp. 267–269. Available at: https://doi.org/10.1088/0508-3443/3/8/306.

Safarian, J. and Tangstad, M. (2009) 'Wettability of silicon carbide by CaO-SiO2 slags', *Metallurgical and Materials Transactions B: Process Metallurgy and Materials Processing Science*, 40(6), pp. 920–928. Available at: https://doi.org/10.1007/s11663-009-9292-5.

T. Fukutake and V. Rajakumar (1982) 'Liquid Packed in the Holdup Beds Dropping and under Abnormal Conditions Flow Phenomena the in Flow Simulating Furnace * Zone of a Blast By Tsuyoshi FUKUTAKE ** and V . RAJAKUMAR ***', *Transactions ISIJ*, 22, pp. 355–364.

Tang, K. and Tangstad, M. (2007) 'Modeling viscosities of ferromanganese slags', *Innovations In The Ferro Alloy Industry - Proceedings of the XI International Conference on Innovations in the Ferro Alloy Industry, Infacon XI*, pp. 344–357.

Tangstad, M. *et al.* (2021) 'Slag Properties in the Primary Production Process of Mn-Ferroalloys', *Metallurgical and Materials Transactions B: Process Metallurgy and Materials Processing Science*, 52(6), pp. 3688–3707. Available at: https://doi.org/10.1007/s11663-021-02347-8.